Solar Physics
DOI: 10.1007/•••••-•••-•••-••••-•

Estimating flare-related photospheric Lorentz force vector changes within active regions

G.J.D. Petrie

© Springer ••••

Abstract It is shown that expressions for the global Lorentz force associated with a flaring active region derived by Fisher et al. (2012) can be used to estimate the Lorentz forces for strong fields in large structures over photospheric subdomains within active regions. Gary's (2001) model for the stratified solar atmosphere is used to demonstrate that in large-scale structures with typical horizontal magnetic length scale >> 300 km and with strong magnetic fields ($\geq$ 1 kG at the $\tau = 1$ opacity layer at 5000 Å), the Lorentz force acting on the photosphere may be approximated by a surface integral based on photospheric boundary data alone. These conditions cover many of the sunspot fields and major neutral lines that have been studied using Fisher et al.'s expressions over the past few years. The method gives a reasonable estimate of Lorentz force changes associated with a flare based on photospheric magnetogram observations provided that the Lorentz force changes associated with the flare have a lasting effect on the observed fields, and are not immediately erased by post-flare equilibration processes.

1. Introduction

In recent years it has repeatedly been shown that the solar photosphere responds to the abrupt coronal reconfiguration of most major flares, often with abrupt, coherent, permanent, and widely distributed patterns of photospheric magnetic field change. Flare-related photospheric magnetic field changes were sought for many years (e.g., Severny, 1964; Zirin and Tanaka, 1981), before abrupt, permanent photospheric field changes were successfully observationally linked to flares; see the discussion in Sudol and Harvey (2005). Since the launch of NASA's Solar Dynamics Observatory (SDO) satellite (Pesnell et al. 2012), the Helioseismic and Magnetic Imager (HMI) instrument (Schou et al. 2011) has provided full-disk vector magnetograms with 0.″5 pixels every 12 minutes, enabling the study of flare-related photospheric vector magnetic field changes in more detail than was possible previously.

National Solar Observatory, Tucson, AZ 85719, USA email:
gpetrie@nso.edu

arXiv:1403.6156v1 [astro-ph.SR] 24 Mar 2014

The history of flare-related photospheric magnetic field changes has not been straightforward. Following the groundbreaking work of Wang et al. (1992, 1994), reporting abrupt, permanent field changes in flaring active regions, a number of later studies produced inconclusive results; see the discussion in Wang (2006). Then, the introduction of high-cadence longitudinal (line-of-sight) photospheric magnetic field measurements, from NASAs Michelson Doppler Imager (MDI) on the Solar and Heliospheric Observatory (SoHO) satellite and the National Solar Observatorys Global Oscillations Network Group (GONG) ground-based network, resulted in mounting evidence of flare-related magnetic changes in the photosphere. Based on one-minute MDI longitudinal data, Kosovichev and Zharkova (1999, 2001) reported sudden and permanent decreases in magnetic flux near X-class flares near magnetic neutral lines, and Zharkova et al. (2005) found a permanent and significant increase in magnetic flux near the neutral line of a region during another X-class flare observed near the limb. Using one-minute GONG longitudinal magnetograms, Sudol and Harvey (2005) characterized the spatial distribution, strength, and rate of change of permanent field changes associated with 15 X-class flares. By carefully co-registering the images they succeeded in tracing the field changes pixel-by-pixel and were able to show the spatial structure of the changes. They concluded that the majority of field changes occurred close to or within sunspots. Wang (2006) found an unshearing movement parallel to the neutral lines in flare-related longitudinal magnetic field changes in the MDI data for all five -spot flares that he studied, implying an overall release of shear, but that the two polarities converged toward the neutral line during some events and diverged during others. Petrie and Sudol (2010) analyzed 1 minute GONG longitudinal magnetograms covering 77 flares of GOES class at least M5 and, exploring the relationship between increasing/decreasing longitudinal fields and azimuth and tilt angles at various positions on the disk, found that the overall distributions of longitudinal increases and decreases at different parts of the disk was found to be consistent with the coronal implosion interpretation (Hudson, 2000; Hudson, Fisher, and Welsch, 2008; Fisher et al., 2012) where, after a coronal magnetic eruption, the remaining coronal field loop structure contracts downward resulting in a more horizontal photospheric field.

Wang and Liu (2010) studied 11 X-class flares using vector magnetograms from the vector magnetograph of Big Bear Solar Observatory and other vector magnetographs, and found in each case an increase of transverse field at the main polarity-inversion line. The launch of SDO and the release of 12-minute HMI photospheric vector magnetograms prompted many authors to study flare-related photospheric vector field changes. Wang et al. (2012), Gosain (2012), Sun et al. (2012) and Petrie (2012, 2013) analyzed the 12-minute HMI vector data for the 15 February 2011 X2.2 flare using different methods, and again found an increase of transverse field at the polarity-inversion line, as did Liu et al. (2012) for the 2011 February 13 M6.6 flare. These observations support Hudson, Fisher, and Welschs (2008) loop-collapse scenario.

Hudson, Fisher, and Welsch (2008) and Fisher et al. (2012) developed a method for estimating the Lorentz force change acting on the photosphere from the atmosphere above using the changes in the photospheric vector field observed

during (or shortly before and after) the flare. The Lorentz force is estimated by integrating components of the Maxwell stress tensor across the boundary of a large domain containing the active region (see Figure 1 of Fisher et al. 2012). The bottom boundary of the domain is identified with the photospheric layer from which the observations derive, and the field values on this boundary are represented by the observations. Because the field values at the lateral and top boundaries of the domain are not measured, Fisher et al. advocated applying their method only to domains where these boundaries are far enough away from the region that the fields crossing them are too weak to contribute significantly to the integral, allowing one to ignore them. Strict adherence to this approach eliminates the possibility of studying the diverse responses of distinct components of an active region, such as sunspots and neutral-line arcades, whose behavior may provide important clues regarding the physics of the flare. Because of this, some authors have proceeded to apply Fisher et al.'s equations to subdomains within active regions (e.g., Wang et al. 2012, Petrie 2012, 2013), sometimes providing brief arguments in favor of doing so (Petrie 2013, Alvarado-Gómez 2012). In particular, it has been argued that the force-free nature of the coronal magnetic field allows one to neglect most of the contribution from the lateral and top boundaries of such a domain. In this paper we will revisit this problem using a model for the stratified solar atmospheric field.

When the 12-minute HMI vector data became available it became possible to apply Fisher et al.s (2012) surface integrals for the photospheric Lorentz force, and it is noteworthy that these calculations have produced strikingly consistent results. Wang et al. (2012) found that the vertical Lorentz force changes associated with 18 major flares were generally directed downward near neutral lines and were correlated with peak soft X-ray flux. Petrie (2012) studied abrupt changes in both the photospheric magnetic and Lorentz force vector associated with six major neutral-line flares using HMI vector data. During all six flares the neutral-line field vectors became stronger and more horizontal, in each case almost entirely due to strengthening of the horizontal field components parallel to the neutral line. In all cases the neutral-line pre-flare fields were less tilted than the reference potential fields, and collapsed abruptly and permanently closer to potential-field tilt angles, implying that the relaxation of magnetic stress played a leading role in creating the magnetic changes. Indeed, the vertical Lorentz force had a large, abrupt, permanent downward change at the main neutral line during each of the flares, consistent with loop collapse. The horizontal Lorentz force changes acted mostly parallel to the neutral line in opposite directions on each side, a signature of the fields contracting during this loop collapse, pulling the two sides of the neutral line toward each other. The greater effect of the flares on field tilt than on shear may be explained by photospheric line-tying, since shear cant be removed during loop collapse without the foot-points moving across the photosphere. Petrie (2013) found that, in the case of the 15 February 2011 X2.2 flare, the oppositely-directed horizontal Lorentz force changes acting on each side of neutral line were accompanied by abrupt torsional un-twisting forces in the two sunspots at each end of the neutral line.

While these studies exploited Fisher et al.s (2012) equations to offer more physical insight into the flare-related magnetic changes than the magnetic vector

information alone, it remained true that Fisher et al. (2012) did not advocate applying their method to fields within active regions and that a detailed defense was lacking. The purpose of this paper is to investigate whether and under what circumstances Lorentz force estimates within active regions can be reliably produced using this method. In this paper we revisit Fisher et al.'s calculation in the context of Gary's (2001) well-known model for the plasma β (the ratio between the plasma and magnetic pressures) of an active region. This allows us to study the influence of solar atmospheric stratification on Lorentz-force distribution between the photosphere and the corona.

The paper is organized as follows. In Section 2 we review Fisher et al.'s (2012) method. In Section 3 we derive expressions representing the contributions to the Lorentz force integral from the different boundary surfaces of a subdomain within an active region, and arrive at inequalities describing conditions where photospheric Lorentz forces within active regions can be derived from photospheric measurements alone. In Section 4 we introduce Gary's (2001) plasma β model and in Section 5 we estimate force contributions from different atmospheric layers using this model. In Section 6 we arrive at conclusions regarding the application of Fisher et al.'s method to subdomains within active regions.

2. Fisher et al.'s (2012) method for estimating photospheric Lorentz force associated with a flaring active region

We briefly summarize the method of Fisher et al. (2012) to estimate the total Lorentz force vector change acting on the photosphere and subphotospheric volume below an active region as a result of a flare. The Lorentz force per unit volume $\mathbf{f}_L$ can be written as,

$$\mathbf{f}_L = \nabla \cdot \mathbf{T} = \frac{\partial T_{ij}}{\partial x_j}, \tag{1}$$

where the Maxwell stress tensor $[T_{ij}]$ in local Cartesian coordinates in terms of the spherical field components (B_r, B_θ, B_ϕ) is,

$$\mathbf{T} = \frac{1}{8\pi}\begin{bmatrix} B_r^2 - B_\theta^2 - B_\phi^2 & 2B_rB_\theta & 2B_rB_\phi \\ 2B_rB_\theta & B_\theta^2 - B_r^2 - B_\phi^2 & 2B_\theta B_\phi \\ 2B_rB_\phi & 2B_\theta B_\phi & B_\phi^2 - B_r^2 - B_\theta^2 \end{bmatrix}. \tag{2}$$

Fisher et al. (2012) evaluated the total Lorentz force over an atmospheric volume surrounding an isolated flaring active region by integrating Equation (1) over this volume, whose lower boundary is identified with the photosphere, with upper boundary far above the photosphere, and side boundaries connecting these surfaces to form a closed volume V as shown in Figure 1 of Fisher et al. (2012). Evaluating the volume integral of Equation (1) using Gauss's divergence theorem then gives (Fisher et al. 2012),

$$\mathbf{F}_L = \int_V \nabla \cdot \mathbf{T}\, \mathrm{d}V = \int_{A_{\mathrm{tot}}} \mathbf{T} \cdot \hat{\mathbf{n}}\, \mathrm{d}A, \tag{3}$$

where the area integral is evaluated over all surfaces of the volume, denoted by $A_{\rm tot}$, with unit normal vector $\hat{\mathbf{n}}$. As Fisher et al. (2012) argue, if the upper boundary of the volume is far enough above the photosphere and the side boundaries are distant enough from the active region that the field integrals over these surfaces are negligible, then the surface integral of Equation (3) reduces to an integral over the photospheric lower boundary $A_{\rm ph}$ only. In this case, for the force acting on the volume below the photosphere, $\hat{\mathbf{n}} = \hat{\mathbf{r}}$ and $\mathbf{B} \cdot \hat{\mathbf{n}} = B_r$ and,

$$F_r = \frac{1}{8\pi} \int_{A_{\rm ph}} (B_r^2 - B_{\rm h}^2)\ {\rm d}A, \tag{4}$$

and

$$\mathbf{F}_{\rm h} = \frac{1}{4\pi} \int_{A_{\rm ph}} (B_r \mathbf{B}_{\rm h})\ {\rm d}A, \tag{5}$$

where we have reversed the signs of these expressions compared to Fisher et al.'s Equations (5) and (6) because because we are considering the forces imposed on the photosphere from above instead of the equal and opposite forces on the atmosphere from below (Fisher et al. 2012).

If one sets the total Lorentz-force to zero, the above surface integrals yield well-known expressions for the Lorentz force on the photosphere (Molodensky 1974) that have been used to derive conditions for the force-freeness of measured photospheric magnetic vector fields (Low 1985). These expressions have also been used to compare the forces of measured fields in the low solar satmosphere using photospheric and chromospheric vector magnetograms (Metcalf et al., 1995). Now, assuming that the photospheric vector field is observed over a photospheric area $A_{\rm ph}$ at two times, $t = 0$ before the flare-related field changes begin, and $t = \delta t$ after the main field changes have occurred, the corresponding changes in the Lorentz force vector components between these two times are given by Equations (17) and (18) of Fisher et al. (2012), again with a change of sign:

$$\delta F_r = \frac{1}{8\pi} \int_{A_{\rm ph}} (\delta B_r^2 - \delta B_{\rm h}^2)\ {\rm d}A, \tag{6}$$

and

$$\delta \mathbf{F}_{\rm h} = \frac{1}{4\pi} \int_{A_{\rm ph}} \delta(B_r \mathbf{B}_{\rm h})\ {\rm d}A, \tag{7}$$

where at a fixed location in the photosphere

$$\delta B_{\rm h}^2 = B_{\rm h}^2(\delta t) - B_{\rm h}^2(0)\ , \tag{8}$$

$$\delta B_r^2 = B_r^2(\delta t) - B_r^2(0)\ , \tag{9}$$

$$\delta(B_r \mathbf{B}_{\rm h}) = B_r(\delta t)\mathbf{B}_{\rm h}(\delta t) - B_r(0)\mathbf{B}_{\rm h}(0)\ . \tag{10}$$

3. Estimating Lorentz force changes within a subdomain of an active region

Let us revisit the Lorentz force integral Equation (3), this time considering the contributions not only from $A_{\rm ph}$ but from all of $A_{\rm tot}$, with the components of $\mathbf{T}$ given in Equation (2). In Equation (3), $A_{\rm tot}$ comprises the photospheric boundary $A_{\rm phot}$ plus the lateral boundaries $A_{\rm lat}$ and the top boundary $A_{\rm top}$.

We now consider the case of a regular sub-domain within the active region with lower boundary at the photosphere. According to Equation (3) the contribution to the Lorentz force vector components from a rectangular photospheric sub-domain of horizontal dimensions $l_x \times l_y$ has typical size,

$$F_{\rm phot} = \frac{1}{8\pi}\int_{y=-l_y}^{l_y}\int_{x=-l_x}^{l_x} B^2(x,y,h_0)\mathrm{d}x\mathrm{d}y \approx \frac{B_0^2}{8\pi}.4l_x l_y = \frac{B_0^2}{2\pi}l_x l_y, \qquad (11)$$

where $z = h_0$ is the height of the photospheric layer from where the observations derive, and B_0 is a typical field strength at that height. Here we have represented the Maxwell stress tensor components in Equation (2) by the magnetic pressure alone for simplicity. This approximation neglects the effects of magnetic tension but is likely to give a useful description of the force distribution because both the magnetic pressure and tension forces are proportional to the square of the field strength.

Unlike the photospheric boundary, the lateral boundaries extend to great heights. On the other hand, recall that for a force-free field the components of the Maxwell stress tensor Equation (2) integrate to zero (Molodensky 1974, Low 1985). Above a certain height $z = L$ in the atmosphere we expect the magnetic field to be close enough to a force-free state, or to be weak enough, that its contribution to Equation (3) is negligible compared to the contribution from the fields below $z = L$. Here we will assume that this is true, and we will test this assumption in Section 5 using models for the stratification of the field.

For simplicity we confine our attention to large, coherent magnetic structures where the field components B_i vary over a length scale L_B such that

$$\frac{\partial B_i}{\partial x} \approx \frac{B_i}{L_B}, \quad \frac{\partial B_i}{\partial y} \approx \frac{B_i}{L_B}. \qquad (12)$$

In this case the difference between the Lorentz forces at the two lateral boundaries at $x = -l_x$ and $x = l_x$ at height z has typical size

$$\frac{\Delta_x(B^2)}{8\pi} \approx \frac{2B_{\rm ave}(z)}{8\pi}.\frac{2l_x B_{\rm ave}(z)}{L_B} = \frac{l_x B_{\rm ave}(z)^2}{2\pi L_B}, \qquad (13)$$

where $B_{\rm ave}(z)$ is a typical field strength at any height z. Then, defining L to be the height over which the field has significant Lorentz forces, the typical size of contribution to the surface integral Equation (3) from two opposite lateral boundaries located at $x = \pm l_x$ is,

$$F_{\rm lat} = \frac{1}{8\pi}\int_{z=h_0}^{L}\int_{y=-l_y}^{l_y}\frac{\Delta_x(B^2)}{8\pi}{\rm d}y{\rm d}z$$
$$\approx \frac{l_x l_y}{\pi L_B}\int_{z=h_0}^{L} B_{\rm ave}(z)^2{\rm d}z. \quad (14)$$

The expression for the typical size of the contribution to the surface integral Equation (3) from the pair of lateral boundaries at $y = -l_y$ and $y = l_y$, based on the difference $\Delta_y(B^2)/(8\pi)$ between the Lorentz forces at $y = -l_y$ and $y = l_y$ at height z, is identical. The contributions from the two pairs of lateral boundaries are the same because, from Equations (12), the horizontal magnetic length scale is (approximmately) the same, L_B, in both horizontal directions, and because, from Equation (14), $F_{\rm lat}$ is proportional to both l_x and l_y.

Comparing Equations (11) and (14), the lateral surface contributions are small enough to be neglected if $F_{\rm lat} << F_{\rm phot}$, i.e., if,

$$\frac{I_z(L)}{L_B} << \frac{B_0^2}{2}, \quad (15)$$

where

$$I_z(L) = \int_{z=h_0}^{L} B_{\rm ave}(z)^2{\rm d}z. \quad (16)$$

The comparison in Equation (15) is independent of the horizontal dimensions l_x and l_y of the domain of integration. So long as the magnetic structure is large and coherent enough that the condition Equation (15) is met, the Lorentz force can be approximated neglecting the lateral boundary contributions.

It remains to consider the contribution to Equation (3) from the top boundary at $z = L$, which has typical size

$$F_{\rm top} = \frac{1}{8\pi}\int_{y=-l_y}^{l_y}\int_{x=-l_x}^{l_x} B^2(x,y,L){\rm d}x{\rm d}y \approx \frac{B_{\rm top}^2}{8\pi}.4l_x l_y = \frac{B_{\rm top}^2}{2\pi}l_x l_y, \quad (17)$$

where $B_{\rm top}$ is a typical field strength at the height $z = L$. Therefore, the contribution from the top boundary can be neglected if $F_{\rm top} << F_{\rm phot}$, i.e., if

$$B_{\rm top}^2 << B_{\rm phot}^2. \quad (18)$$

Equations (15) and (18) describe conditions where the lateral and top boundary contributions to the Lorentz force integral Equation (3) are much smaller than the photospheric contributions, and can be neglected, so that the whole-surface integrals can be approximated by the lower boundary integrals alone.

Under these conditions, a reasonable Lorentz force estimate can be performed using photospheric measurements alone. Equations (15) and (18) represent criteria that we will use to test various model fields in Section 5 of the paper.

Clearly, not all fields pass this test. For example, with any force-free field the three components of Equation (3) must be zero, and these integrals therefore cannot possibly have dominant lower boundary contributions; $F_{\rm phot}$ cannot be much larger than both $F_{\rm lat}$ and $F_{\rm top}$. In these cases, therefore, the lateral and top boundary integrals cannot be neglected, and the lower boundary integral cannot accurately represent the whole boundary integral. A good Lorentz force estimate therefore cannot be derived from photospheric measurements alone for force-free fields. To satisfy Equations (15) and (18), the flux distribution must be very different from that of a force-free field: the field strength must fall off sufficiently sharply with height that the photospheric contribution to the force integral Equation (3) is dominant. With flux conservation this means that the field must contain a lot of return flux (escape through the bottom boundary) and/or flux tube expansion (escape through the lateral boundaries). But the details of how the flux escapes from the domain to achieve this stratification are not directly relevant to Equations (15) and (18). The condition imposed by Fisher et al. (2012), that the field integrals over the top and lateral boundaries must be negligible, is a sufficient but not a necessary condition for Equations (15) and (18) to be fulfilled. Equations (15) and (18) can be fulfilled within an active region if the field strength decreases with height fast enough and the lateral boundary pressure differences are not too large. In Section 5 we will use models to determine whether fields can be sufficiently steeply stratified under solar conditions that both of Equations (15) and (18) are satisfied for reasonable horizontal length scales L_B.

Before we introduce models, we can note that the solar atmospheric field strength does indeed fall off sharply according to various observations summarized by Gary (2001), and this is what is needed to satisfy Equations (15) and (18). Metcalf et al. (1995) estimated that the atmosphere is approximately force-free (i.e., much less forced than the photosphere) about 400 km above the photosphere. This result suggests that a box of integration with height $L = 400$ km would capture all significant Lorentz forces. Crudely estimating $I_z(L) \leq B_0^2 L$ from Equation (16), Equation (15) then says that for magnetic structures of characteristic horizontal length scale $L_B >> 2L = 800$ km, the contribution $F_{\rm lat}$ to Equation (3) should be negligible. This crude estimate leads us to expect that many photospheric Lorentz forces may be estimated using photospheric field measurements alone, but it does not adequately take into account the effects of solar atmospheric stratification. Not only does it ignore the effect of the photospheric fields generally being much stronger than most of the fields crossing the lateral boundary, but also the small but finite contributions to the Lorentz forces from fields in and above the chromosphere.

To explore the influence of solar atmosphere stratification on the validity of the result, it is necessary to rely on a model for the stratification of the solar atmospheric field. Current extrapolation solutions are too weakly stratified to reproduce the stratification of the solar atmosphere from the photosphere to the corona. This applies not only to force-free fields that we discussed above,

but also to non-force-free fields. Non-force-free extrapolations are rare, but Hu et al. (2010) presented such a model based on an optimized linear combination of a potential field and two linear force-free fields. This model may represent the Lorentz forces reasonably well at the height of the observations in the photosphere, but not the great differences between the measured photospheric fields and the nearly force-free fields only a few hundred km above. To determine whether Fisher et al.'s equations can give useful estimates of major photospheric Lorentz force changes within active regions using photospheric data, it is essential to represent the solar stratification accurately. We need another approach. In this paper we apply instead the simple and observationally constrained model of solar atmospheric stratification presented by Gary (2001).

4. Gary's (2001) model for the magnetic and plasma stratification above an active region

The solar corona has a complex structure with the plasma pressure and magnetic pressure dominant in different domains. The plasma pressure tends to be very dominant in the solar interior, though this may not be the case in some intense sunspot fields near the surface. The magnetic pressure tends to dominate between the chromosphere and mid-corona, though some atmospheric structures such as weak-field prominences seem likely to have significant plasma forces. In the open-field domain of the high corona the thermal and kinetic pressures of the expanding solar wind dominate the magnetic pressure, forcing the field to open at heights around a solar radius. The dimensionless parameter that characterizes this competition between the magnetic pressure $B^2/8\pi$ and plasma pressure p is the plasma β,

$$\beta = \frac{8\pi p}{B^2}. \tag{19}$$

Generally, $\beta > 1$ in the photosphere and $\beta < 1$ between the chromosphere and mid-corona, and becomes > 1 again around a solar radius above the photosphere (Gary 2001).

Estimates of the relative contributions to the force integral Equation (3) from photospheric compared to non-photospheric heights must account for both the decrease in magnetic field strength as a function of height and the increasing force-freeness of the field as a function of height. Of course the Lorentz force cannot be measured throughout the atmosphere, only at heights where magnetically sensitive spectral lines are formed. Practically, this restricts observational estimates of Lorentz forces to the thin layers of the photosphere up to the chromosphere. The height-dependence of the solar magnetic field is difficult to determine observationally because, while observations of chromospheric and coronal Zeeman lines are becoming more common (e.g., Lin et al. 2000, Tomczyk et al. 2008, Rachmeler et al. 2013), the height of formation of the chromospheric lines can be ambiguous, and projection effects pose problems of interpretation for optically thin corona plasmas. Furthermore, detailed interpretation of asymmetric Stokes profiles is complicated by magnetic gradients and flows. Direct

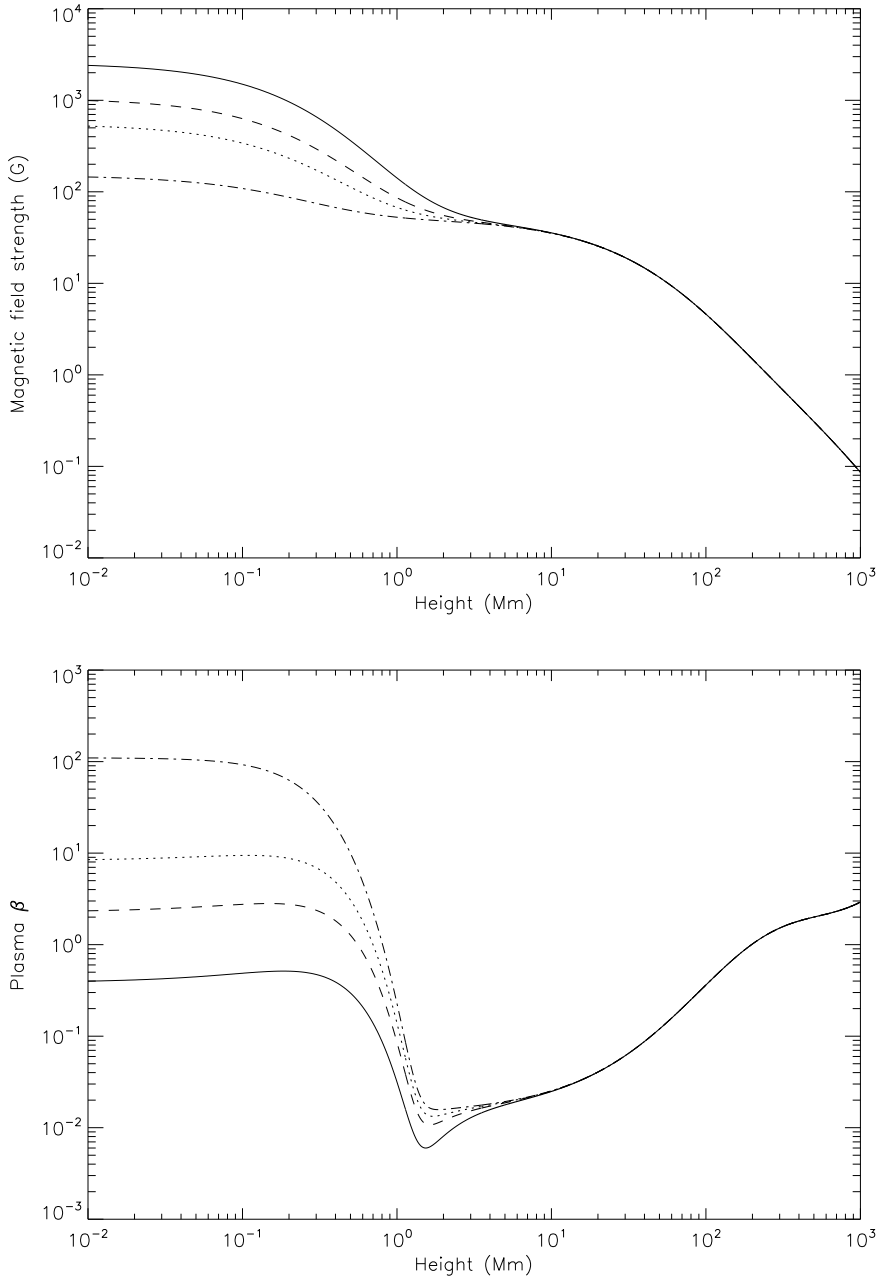

Figure 1. The magnetic field strength (top) and plasma beta (bottom) for four magnetic field models, plotted against height in the solar atmosphere. The solid and dot-dashed lines represent the models for sunspot and plage fields with photospheric field strengths of 2500 G and 100 G presented by Gary (2001). The dashed and dotted lines represent intermediate fields of photospheric field strength 1000 G and 500 G.

measurement of Zeeman splitting can provide tests of inversion methods but only for very strong fields.

The formation height of the Na D line is believed to be about 600 km, a few pressure scale heights above the formation height of the photospheric Fe I lines. From Mees Solar Observatory Na D data Metcalf et al. (1995) estimated a magnetic field gradient of about 0.8-1.1 G km^{-1}, which seems to be a typical estimate for the first Mm above the photosphere (Gary 2001). From prominence magnetic field observations, Harvey (1969) found an exponential field gradient of about 1.6 G km^{-1}, representing a height range of about 10 Mm, above which height the field is believed to decrease in strength more steeply (Gary 2001).

Guided by these observations, Gary (2001) represented the height profile of the sum of parametric dipole terms (Aschwanden et al. 1999),

$$B = B_s \Big/ \left(1 + \frac{z}{H_s}\right)^3 + B_f \Big/ \left(1 + \frac{z}{H_f}\right)^3 + B_w \Big/ \left(1 + \frac{z}{H_w}\right)^3 , \qquad (20)$$

where $H_s = 0.5$ Mm, $H_f = 75$ Mm, and $H_w = 696$ Mm. The parameter B_s imposes a typical field strength in the photosphere, B_f represents the field strength in the mid-corona and B_w the global field strength taking into account the effect of the solar wind. The first term decays rapidly due to the expansion of the field in the chromospheric canopy. Gary (2001) derived upper and lower envelopes for the field model representing sunspot and plage fields using the parameter values $B_s = 2500$ G for the sunspot field and 100 G for the plage field, $B_f = 50$ G for both fields, and $B_w = 1$ G for the sunspot field and 0.005 G for the plage field. Figure 1 shows plots of four models described by Equation (20): the sunspot model (solid curve) the plage model (dot-dash curve) and two intermediate models with photospheric field strengths $B_s = 1$ kG (dashed curve) and 500 G (dotted curve). We have set $B_f = 50$ G and $B_w = 1$ G in all four of our models since these constants represent the mid-coronal and global-coronal field strengths above the same active region in all four cases. We only need to vary B_s to compare the stratification of the sunspot umbral, plage and intermediate fields in our model region.

Equation (20) represents only dipole-like behavior of active region fields whereas active regions often have complex, multipolar photospheric flux distributions. Assuming that a region has approximately balanced magnetic flux and therefore has negligible monopole component, the dipolar component of this flux is the component that decreases most slowly with height and has the largest global influence. The dipole model therefore represents the field of most interest in our study, that most likely to contribute to the lateral and top boundary integrals in a Lorentz force calculation based on Equation (3).

Figure 1 (top) shows how the magnetic field strength $B = |\mathbf{B}|$ varies as a function of height for each of the four magnetic field models. For all four models the magnetic field strength decreases steeply in the first several Mm, showing the dominant influences of the B_s term in the first Mm and of the B_f term from there up to about 75 Mm. We will use these models to estimate the height-dependence of the Lorentz force according to Equation (3).

Gary's (2001) plasma pressure model is formed by a linear combination of barometric terms representing chromospheric and coronal temperature regions,

$$p(z) = p_c e^{-(z/H_c)(R/R_s)} + p_k e^{-(z/H_k)(R/R_s)}, \tag{21}$$

where $R = R_s + z$ is the radial coordinate, the sum of the solar radius R_s and the height z above the solar surface, H_k is the chromospheric scale height, and $H_c = H_0(R/R_s)^2$ is the spatially varying effective coronal scale height corrected for gravity. The parameter values used are $p_c = 1.5$ dyn cm^{-1}, $p_k = 1 \times 10^5$ dyn cm^{-1}, $H_0 = 55$ Mm and $H_k = 0.12$ Mm. This pressure profile was constrained by pressure estimates from Gary & Alexander (1999) derived from Yohkoh/SXT observations above an active region at the limb, and electron number density data corresponding to height 2.5×10^3 Mm at temperature $T = 2$ MK from Allen (1973).

Figure 1 (bottom) shows how the plasma β, the ratio of the plasma and magnetic pressures given by Equation (19), varies as a function of height for each of the four magnetic field models. The plasma β is around 1 (0.8) at the photosphere for the umbral field model (2500 G) and > 1 for the other models. The plage field model has plasma $\beta > 200$ at $z = 0$ Mm. Within 1 Mm all four models have $\beta < 1$. At a height of about 100 Mm all models transition to a $\beta > 1$ regime. This means that there is a layer of the atmosphere in all four models between heights 1 Mm and 100 Mm where the field is dominant over the plasma and, having no significant plasma forces opposing it, is likely to be approximately force-free.

5. Estimating the Lorentz force integral contributions from the different atmospheric layers

The integral P_m of the magnetic pressure over height,

$$P_m = \int_0^z B^2/8\pi \, \mathrm{d}z', \tag{22}$$

gives a crude estimate of the Lorentz force per unit area of the photosphere, approximating the left equality of Equation (3). This integral represents the magnetic pressure only. We ignore for the moment the approximately force-freeness of much of the coronal field, in which the opposition of the magnetic tension force to the magnetic pressure gradient force plays a crucial role. Figure 2 (top) shows how this integral varies as a function of height for each of the four magnetic field models. In each case P_m increases monotonically to an asymptotic value at great heights but the rate of increase is different for the four field models. Whereas for the umbral field model P_m integrated up to 1 Mm almost matches its integral up to 1000 Mm, for the plage field model there is a an order of magnitude difference between the P_m integrals for the two heights. This suggests that the contribution to the magnetic pressure integral P_m integral above around 1 Mm may be negligible in the case of umbral fields but not for plage fields. For the

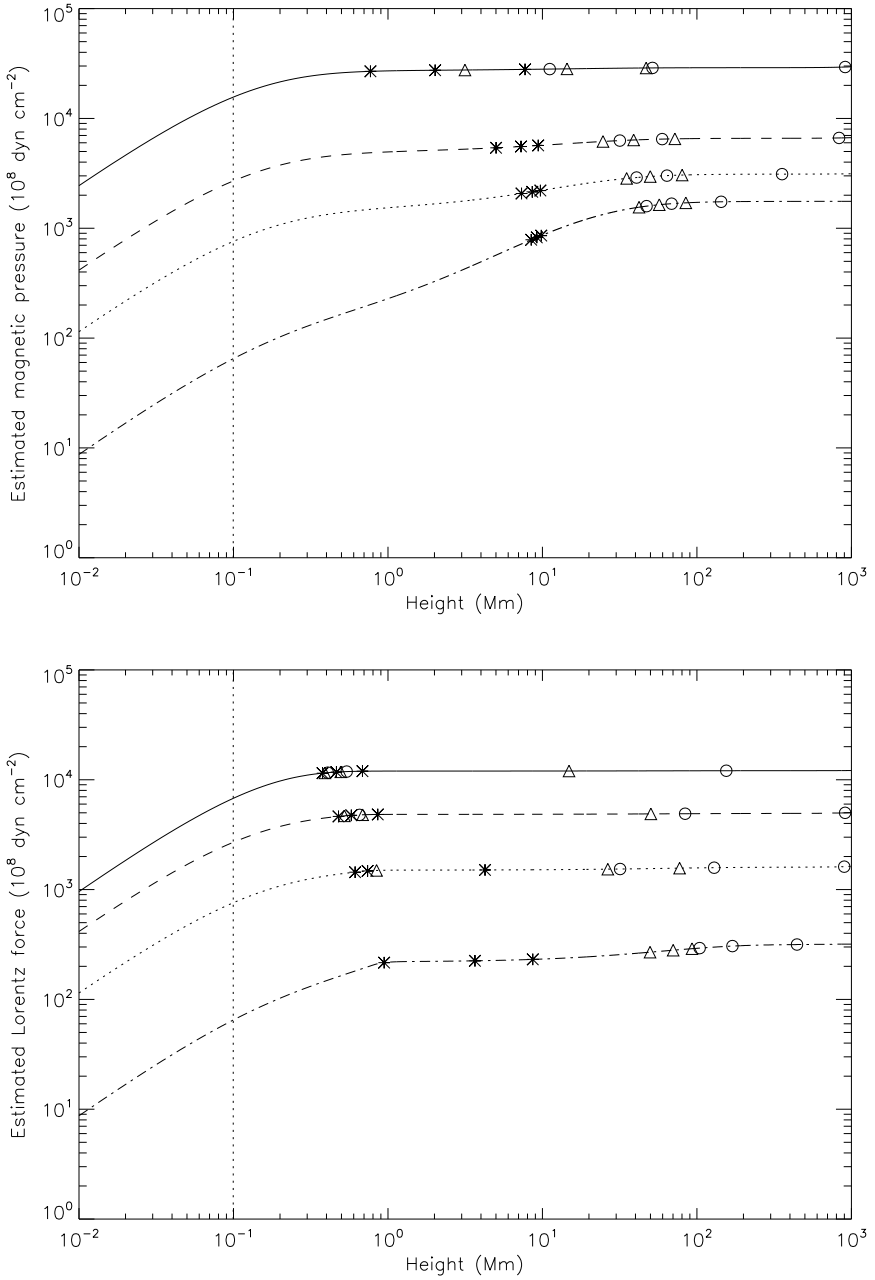

Figure 2. The integrated magnetic pressure (top) and simulated Lorentz force density (bottom) for the four magnetic field models, plotted against height in the solar atmosphere. These quantities are integrated from $z = 0$ to the heights indicated (see Equations (22) and (24)), giving profiles that increase with height and become flat at great heights. For each model, the Lorentz force is estimated using the plasma pressure and β as in Equation (24). The solid and dot-dashed lines represent the models for sunspot and plage fields with photospheric field strengths of 2500 G and 100 G presented by Gary (2001). The dashed and dotted lines represent intermediate fields of photospheric field strength 1000 G and 500 G.

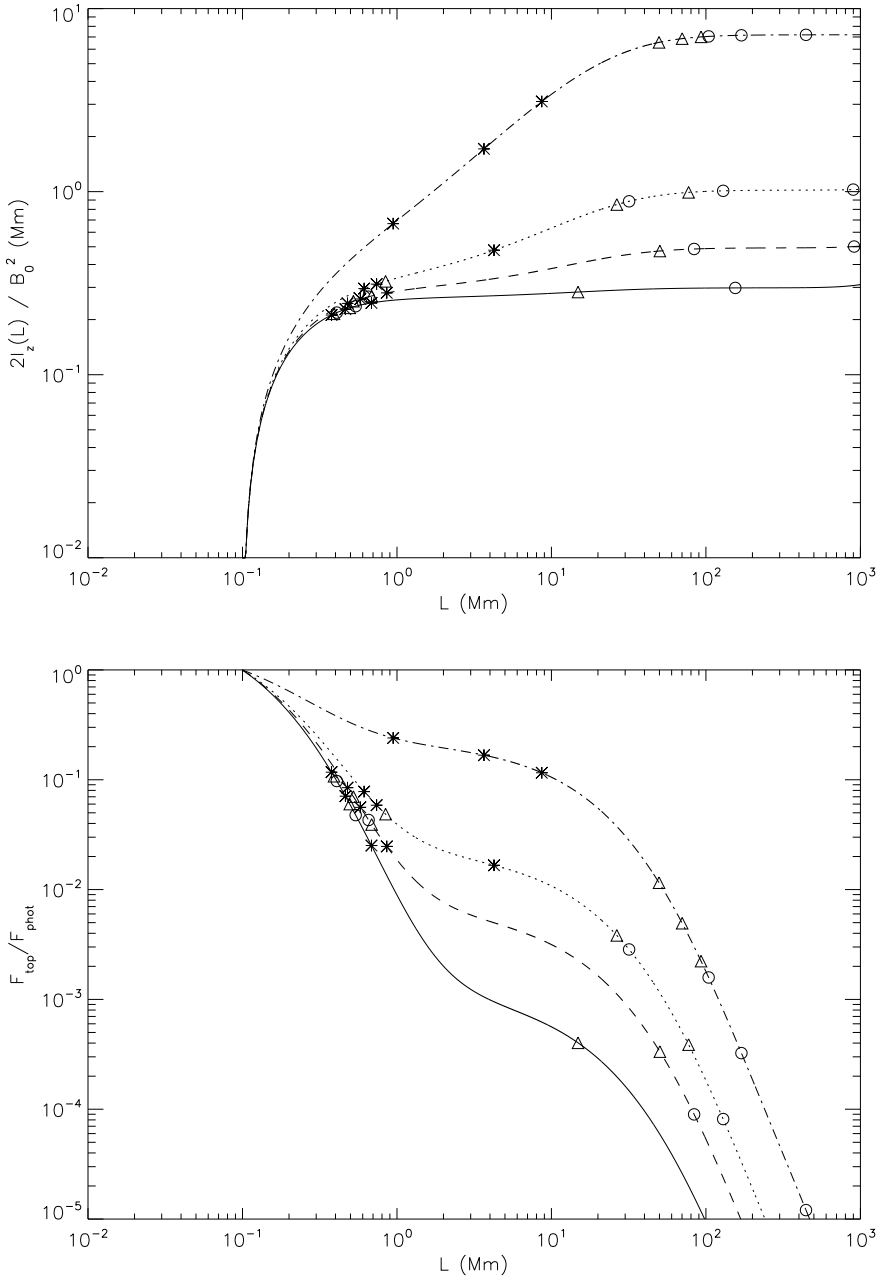

Figure 3. Comparison of the contributions from the photospheric boundary and the lateral boundaries (top) and comparison of the contributions from the photospheric boundary and the top boundary (bottom), plotted against top boundary heights L. The solid and dot-dashed lines represent the models for sunspot and plage fields with photospheric field strengths of 2500 G and 100 G presented by Gary (2001). The dashed and dotted lines represent intermediate fields of photospheric field strength 1000 G and 500 G. In the top plot, for a given model and top boundary heights L, the field's horizontal length scale L_B would have to be significantly larger than the value plotted for the lateral boundary contributions to be negligible. In the bottom plot the top boundary contribution is negligible wherever the curve is much less than one.

intermediate field models there are significant contributions to the P_m integral up to about 10 Mm.

Here $z = 0$ represents the height where the opacity $\tau = 1$ at 5000 Å, the usual definition of the photospheric surface. The vertical dotted lines in Figure 2 indicate the approximate height $z = 100$ km in the photosphere from where typical HMI observations derive according to Fleck et al. (2011). From correlations between simulated Doppler velocities and derived Dopplergrams, Fleck et al. concluded that the HMI observations of the Fe I 6173 Å line originate from heights lower than the line core formation height, about 100 km. They found a similar result for the MDI signal, around 125 km, for the Ni I line at 6768 Å also used by GONG. One may expect a similar result for the Fe I line at 6302.5 Å used by Hinode and the NSO Synoptic Optical Long-term Investigations of the Sun (SOLIS) Vector Spectro-magnetograph (VSM), though the calculation has not been performed for this line. Fleck et al. also estimated that smearing effects associated with the instrumentation make the fine structure in the images appear to correspond to heights about 40-50 km higher in the photosphere. However, for the large, well resolved magnetic structures that we are considering, sunspot and neutral-line structures much larger than the HMI pixel size $0\farcs5$, the smearing effect is unlikely to be important. We therefore adopt the height $h_0 = 100$ km as the photospheric boundary for our Lorentz force estimates. We repeated the following analysis with the value $h_0 = 125$ km and found similar results.

Over-plotted on each curve in Figure 2 (top) are three asterisks, three triangles and three circles. The three asterisks on each curve represent the heights L where

$$\frac{1}{8\pi}\int_{z=h_0}^{L} B^2 \mathrm{d}z = \frac{C}{8\pi}\int_{z=L}^{h_1} B^2 \mathrm{d}z, \tag{23}$$

for the three cases with $C = 0.9$, 0.95 and 0.99, and $h_1 = 10$ Mm. This value of h_1 corresponds to the typical height of a flare hard X-ray (HXR) source found in a statistical study of YOHKOH data by Matsushita et al. (2002). Thus, on each curve, the first asterisk indicates the height $z = L$ where 90% of the total magnetic pressure between the height of the HMI observations ($z = h_0$) and the height of a typical HXR source ($z = h_1 = 10$ Mm) is confined to heights below $z = L$. The second and third asterisks show the heights L that contain 95% and 99% of the magnetic pressure. The three triangles show the equivalent heights L for $h_1 = 100$ Mm, a typical heigh of a tall active region loop. The three circles show the equivalent heights L for $h_1 = 1000$ Mm, which roughly represents the height high in the corona where the expanding solar wind dominate the magnetic field. The plot shows that, while most of the magnetic pressure associated with each of the four models is concentrated low in the atmosphere, L needs to be at least several Mm in size for any but the strongest field models to concentrate more than 90% of the magnetic pressure below $z = L$.

The magnetic pressure surely overestimates the size of the Lorentz force in the corridor between about $z = 1$ Mm and 100 Mm where the plasma $\beta < 1$ and the field is likely to be approximately force-free, with the magnetic pressure gradient force opposed by the magnetic tension force. To estimate the effect of

this force-freeness on the Lorentz force integral in Equation (22) we modify the integral,

$$L_f = \int_0^z \beta_{<1} B^2/8\pi \, \mathrm{d}z', \tag{24}$$

using the factor

$$\beta_{<1} = \begin{cases} \beta & \text{wherever } \beta < 1 \\ 1 & \text{wherever } \beta \geq 1 \end{cases}$$

to simulate the varying influence of force-freeness as a function of height. This forces the integrand of Equation (24) to equal the magnetic pressure $B^2/8\pi$ where $\beta < 1$ and the plasma pressure p where $\beta > 1$. The reason for defining Equation (24) in this way is as follows. If $\beta > 1$ then the magnetic field is dominated by the plasma so that the magnetic forces have the typical size $B^2/8\pi$ of the magnetic pressure. If $\beta < 1$ then the magnetic field dominates the plasma, and much of the Maxwell stress is contained within the magnetic field: the magnetic pressure gradient can be opposed not only by the plasma pressure gradient but also by the magnetic tension force. The resulting Lorentz force is then smaller than the magnetic pressure force. Since the plasma pressure gradient force is expected to balance this Lorentz force we set these forces to have equal size wherever $\beta < 1$. In cases with $\beta \ll 1$ the magnetic pressure and tension forces almost cancel and the field is approximmately force-free. We model this relationship between low plasma-β values and the force-freeness of the field using the factor $\beta_{<1}$ in Equation (24).

This simple model for the Lorentz force does not capture the complexity of force vectors in active regions. It is designed to describe the general size of the Lorentz force at different heights. In reality the direction of this vector can become an important consideration. For example, if a component of the Lorentz force vector becomes small at some location in the photosphere then contributions to Equation (3) from higher in the atmosphere might become significant at this location. However, such contributions would be small compared to the contributions from the photosphere generally and would not obscure the overall photospheric Lorentz force pattern.

Figure 2 (bottom) shows how this modified integral Equation (24) for the integrated Lorentz force L_f varies as a function of height for each of the four magnetic field models, and comparing the two panels of Figure 2 reveals the effect of the varying plasma β. The integrals have become slightly smaller and the curves between $z = 1$ Mm and 100 Mm, where the plasma $\beta < 1$, are significantly flatter for the L_f integrals (bottom panel) than for the P_m integrals (top panel). The contributions to the L_f integral Equation (24) from the nearly force-free fields between these heights is small enough to be negligible for the umbral model and the intermediate 1000 G model. For the 500 G model the integral up to 1 Mm is about 90% of the integral up to 100 Mm.

Figure 2 (bottom) also shows three asterisks, triangles and circles on each curve. These symbols correspond to heights L where,

$$\frac{1}{8\pi}\int_{z=h_0}^{L}\beta_{<1}B^2\mathrm{d}z = \frac{C}{8\pi}\int_{z=L}^{h_1}\beta_{<1}B^2\mathrm{d}z, \tag{25}$$

where $h_1 = 10$ Mm (asterisks), 100 Mm (triangles), and 1000 Mm (circles), and the three symbols in each case represent $C = 0.9$, 0.95 and 0.99 as in the top panel of Figure 2 discussed above. It is clear from the bottom plot that, taking into account only fields up to 10 Mm (asterisks), over 90% of the estimated Lorentz force is concentrated in $h_0 \leq z \leq L$ with $L \approx 1$ Mm for all four models. If we relax our conditions to include all fields up to 100 M (triangles), then we still capture over 90% of the estimated Lorentz forces within $h_0 \leq z \leq L$ with $L < 1$ Mm for the three strongest models, excluding only the model for plage fields (dot-dashed curve). If we consider all fields up to 1000 Mm then the two strongest models still contain more than 90% of their estimated Lorentz forces within the layer $h_0 \leq z \leq L$ with $L \approx 1$ Mm. For $h_1 = 100$ Mm over 95% of the two strongest models' estimated Lorentz forces are contained within $h_0 \leq z \leq L$ with $L \approx 1$ Mm, and for $h_1 = 10$ Mm this percentage goes up to over 99%. These results indicate that if we set $L \approx 1$ Mm and neglect all Lorentz force contributions above that height, then we can expect to miss less than 10% associated with active region loops with > 500 G photospheric fields (i.e., > 500 G at the $\tau = 1$ opacity surface at 5000 Å), and less than 5% for loops with > 1 kG fields. A value $L \approx 1$ Mm therefore seems to be suggested by these considerations. Now we need to check the sizes of the contributions to Equation (3) from the different boundaries as discussed in Section 3.

Figure 3 allows a visual comparison between the contributions to the Lorentz force surface integral Equation (3) from the photospheric boundary and the lateral boundaries (top plot) and the top boundary (bottom plot). The top plot shows the quantity $2I_z(L)/B_0^2$ for each of the four field models as a function of top boundary height L. For any value of L, the horizontal magnetic spatial scale L_B of the structure must be comfortably larger than this quantity if the lateral boundary contribution F_{lat} is to be negligible - see Equation (15). The three asterisks, triangles and circles per curve in Figure 3 (top) represent the values of L shown in Figure 2 (bottom) for the estimated Lorentz force. The cluster of symbols near and below $L = 1$ Mm is concentrated between values $2I_z(L)/B_0^2 = 200$ km and 300 km. The plot therefore shows that for the size of $L \approx 1$ Mm discussed above, L_B must be significantly larger than 200 km or 300 km. Since this scale is significantly smaller than the typical length scales of the sunspots and major neutral lines generally studied using this method (e.g., Wang et al. 2012, Petrie 2012, 2013), this result indicates that the contributions to Equation (3) from the lateral boundaries, F_{lat}, can be neglected for such structures, particularly those whose fields have strength corresponding to the two strongest models ($|\mathbf{B}| \geq 1$ kG at $z = 0$).

Figure 3 (bottom) shows the ratio between the top and photospheric boundary contributions to Equation (3), $F_{\mathrm{top}}/F_{\mathrm{phot}}$, as a function of top boundary height L for each model. For values of L where this ratio is $<< 1$, the contribution F_{top} to Equation (3) can be neglected. The three asterisks, triangles and circles per curve in this plot again represent the values of L shown in Figure 2 (bottom) for the

estimated Lorentz force. For the cluster of symbols near and below $L = 1$ Mm, the ratio $F_{\rm top}/F_{\rm phot}$ is between 10^{-2} and 10^{-1}, indicating that the contribution $F_{\rm top}$ can also be neglected from estimates based on Equation (3) for our magnetic structures of interest.

There is some tension between Equations (15) and (18) which can be seen by comparing the two plots of Figure 3. One of the ratios plotted in the figure cannot decrease without the other increasing: if the upper boundary height L increases, the top boundary integral decreases but the lateral boundary integral must increase. On the other hand, stratification supports both inequalities in the same way, concentrating the forces near the lower boundary and making the lower boundary integral bigger. The most stratified models (solid and dashed lines) therefore have the smallest ratios in both panels of Figure 3.

In Figure 3 we have again represented the Maxwell stress tensor Equation (2) by the magnetic pressure. The symbols of interest in Figure 3 appear at heights below $z = 1$ Mm and mostly correspond to plasmas with $\beta > 1$, where the magnetic pressure gradient likely represents the size of the Lorentz force reasonably well. In the strongest models β becomes < 1 at heights $z < 1$ Mm. In these cases the Lorentz force likely becomes smaller than the magnetic pressure gradient where $\beta < 1$ because the magnetic tension generally must help the plasma pressure gradient force to oppose the magnetic pressure gradient force. Since this effect becomes larger as the height increases, the fall-off of the Lorentz force with height is therefore likely to be underestimated for the strongest models shown in Figure 3. However, the equivalent plots of Figure 3 with B^2 replaced by $\beta_{<1}B^2$ (not shown) produced little effect on the cluster of symbols near $L = 1$ Mm, suggesting that our simple model based on the magnetic pressure $B^2/8\pi$ adequately represents the Maxwell stress tensor within the height range of interest.

6. Conclusion

We conclude that for strong magnetic fields the contribution to the Lorentz force estimate from fields at height above around 1 Mm can be neglected. For photospheric subdomains filled with large, coherent structure and strong magnetic field, the contributions to the surface integrals derived by Fisher et al. (2012) are negligible compared to the contribution from the photospheric boundary. This implies that Fisher et al.'s (2012) method for estimating Lorentz force changes on the photosphere during solar flares using Equations (4) and (5) can be applied to subdomains within a a flaring active region, so long as the conditions on strength of field and coherence of structure are met within this photospheric subdomain. For HMI data, and for data originating from similar heights in the solar atmosphere, the horizontal length scale of the structure needs to be much larger than 500 km and the field needs to be stronger than about 630 G at the height of the observations ($\geq$ 1 kG at the $\tau = 1$ opacity layer at 5000 Å). This conclusion therefore supports many of the published surface integral calculations based on Fisher et al.'s method, such as those by Petrie (2012,2013), who used regular rectangular integration domains covering

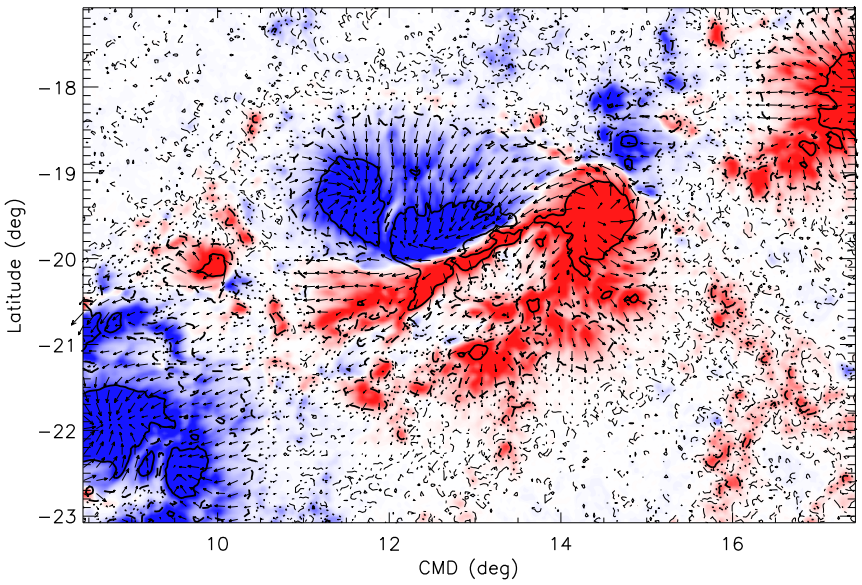

Figure 4. Vector magnetic field before the 2011 February 15 X2.2 flare. The vertical field component, Br, is indicated by the color scale and the horizontal component by the arrows, with saturation values 1000 G. Red/blue coloring represents positive/negative vertical field. The solid, dashed, dotted and dot-dashed contours indicate photospheric field strengths corresponding to the four models featuring in the previous figures and described in Section 4. At the approximate height of the HMI observations, $z = 100$ km, these models have field strength 1500 G, 629 G, 340 G and 108 G, respectively.

strong neutral line fields and circular domains covering sunspots, and Wang & Liu (2010), Wang et al. (2012), who used irregular domains covering strong sunspot and neutral line fields. Figure 4[1] shows the much-studied HMI vector magnetic field associated with the 2011 February 15 X2.2 flare. The plot shows that most of the important fields at the heart of the active region NOAA 11158 are strong enough to meet the above conditions, and the major features of the region have horizontal spatial scale much larger than 500 km.

Note that Fisher et al.'s equations record only the Lorentz force difference between two vector magnetogram measurements covering the same locations at different times. During a highly dynamic event such as a flare, Lorentz forces apply to different layers of the solar atmosphere, but only those layers whose fields have significant and steady Lorentz force values before and after the flare will yield measurements that can be analyzed using this method. In a nearly force-free layer of the atmosphere the magnetic vectors may respond strongly to

[1]This figure is updated from Figure 1 of Petrie (2012). In Petrie (2012) the longitude-latitude coordinate system has origin at the center of the remapped HMI magnetogram whereas here the origin corresponds to disk-center.

a flare. However, if the magnetic vector field in this layer is not associated with significant Lorentz forces before and after the flare then Equations (6) and (7) for the Lorentz force change will not give a result that can be understood as a flare-related Lorentz force vector change. This is true even if the flare produced a large and permanent change in the magnetic vector field. In some nearly force-free layers of the solar atmosphere, dynamical equilibration processes remove any significant Lorentz forces from field configurations, erasing all traces of the Lorentz force changes produced by flares. It is therefore essential to the success of this method that the magnetogram observations derive from a layer where such force-removing equilibration processes do not generally occur.

Acknowledgements This project was prompted by discussions at Leverhulme Flare Seismology Workshop held at the Mullard Space Science Laboratory (MSSL), 9-12 September 2013. The author thanks the Leverhulme trust for hospitality during the author's visit to MSSL, and thanks his fellow participants at the workshop for interesting discussions during and after the meeting.

References

Alvarado-Gómez, J.D., Buitrago-Casas, J.C., Martínez-Oliveros, J.C., Lindsey, C., Hudson, H. & Calvo-Mozo, B.: 2012, *Solar Phys.* **280**, 335
Fleck, B., Couvidat, S. & Straus, T.: 2011, *Solar Phys.* **271**, 27
Fisher, G.H., Bercik, D.J., Welsch, B.T. & Hudson, H.S.: 2012, *Solar Phys.* **277**, 59
Gosain, S.: 2012, *Astrophys. J.* **749**, 85
Hu, Qiang, Dasgupta, B., Derosa, M. L., Büchner, J., Gary, G. A.: 2010, *Journal of Atmospheric and Solar-Terrestrial Physics* **72**, 219
Hudson, H.S.: 2000 *Astrophys. J.* **531**, L75
Hudson, H.S., Fisher, G.H. & Welsch, B.T.: 2008, in *Subsurface and Atmospheric Influences in Solar Activity*, ASP Conf. Series 383, 221
Kosovichev, A.G., & Zharkova, V.V.: 1999, *Sol. Phys.* **190**, 459
Kosovichev, A.G., & Zharkova, V.V.: 2001, *Astrophys. J.* **550**, L105
Lin, H., Kuhn, J.R., Coulter, R.: 2004, *Astrophys. J.* **613**, L177
Low, B.C.: 1985, In: Hagyard, M.J. (ed.) *Measurements of Solar Vector Magnetic Fields*, NASA, Huntsville, 49
Matsushita, K., Masuda, S., Kosugi, T., Inda, M. & Yaji, K.: 1992, *Pub. Astron. Soc. Japan***44**, 89
Metcalf, Thomas R., Jiao, Litao, McClymont, Alexander N., Canfield, Richard C., Uitenbroek, Han: 1995, *Astrophys. J.* **439**, 474
Molodensky, M.M.: 1974, *Solar Phys.* **39**, 393
Petrie, G. J. D.: 2012, *Astrophys. J.* **759**, 50
Petrie, G. J. D.: 2013, *Solar Phys.* **287**, 415
Petrie, G. J. D., Sudol, J. J.: 2010, *Astrophys. J.* **724**, 1218.
Rachmeler, L. A., Gibson, S. E., Dove, J. B., DeVore, C. R., Fan, Y.: 2013, *Solar Phys.* **288**, 617
Schou, J., Scherrer, P.H., Bush, R.I., et al.: 2011, *Solar Phys.*, doi: 10.1007/s11207-011-9842-2
Severny, A.B.: 1964, *Ann.Rev Astron. Astrophys.* **2**, 363
Sudol, J.J. & Harvey, J.W.: 2005, *Astrophys. J.* **635**, 647
Tomczyk, S., Card, G.L., Darnell, T., Elmore, D.F., Lull, R., Nelson, P.G., Streander, K.V., Burkepile, J., Casini, R., Judge, P.G.: 2008, *Solar Phys.* **247**, 411
Wang, H.: 2006, *Astrophys. J.* **649**, 490
Wang, H., Ewell, M.W., Zirin, H. & Ai, G.: 1994, *Astrophys. J.* **424**, 436
Wang, H. & Liu, C.: 2010, *Astrophys. J.* **716**, L195
Wang, H., Varsik, J., Zirin, H., Canfield, R.C., Leka, K.D., & Wang, J.: 1992, *Solar Phys.* **142**, 11

Wang, S., Liu, C., Liu, R., Deng, N., Liu, Y. & Wang, Haimin: 2012, *Astrophys. J.* **745**, L17
Zharkova, Valentina V., Zharkov, Sergey I., Ipson, Stanley S., Benkhalil, Ali K.: 2005, *J. Geophys. Res.* **110**, A08104
Zirin, H., & Tanaka, K.: 1981, *Astrophys. J.* **250**, 791